Observation and implications of magnetic domains in lateral spin valves

J. Mennig, F. Matthes, D. E. Bürgler, and C. M. Schneider

Additional information on J. Appl. Phys.

Observation and implications of magnetic domains in lateral spin valves

J. Mennig, F. Matthes, D. E. Bürgler,[a] and C. M. Schneider
Peter Grünberg Institute, Electronic Properties (PGI-6) and Jülich-Aachen Research Alliance,
Fundamentals of Future Information Technology (JARA-FIT), Forschungszentrum
Jülich GmbH, Jülich D-52425, Germany

Co/Cu/Co lateral spin valves (LSV), with Co being the topmost layer, are *in situ* prepared and measured under ultrahigh vacuum conditions. The clean process yields a non-local spin signal of 0.9 mΩ. Scanning electron microscopy with polarization analysis (SEMPA) reveals domain structures in both magnetic electrodes that depend on the LSV dimensions. The spin signal correlates to SEMPA images as well as the anisotropic magnetoresistance of both Co magnets, revealing a strong impact of multi-domain states on the spin signal. © *2012 American Institute of Physics*. [doi:10.1063/1.3671415]

Current developments in spintronics address pure spin currents, which are envisaged to enable spintronic devices free from adverse charge-related effects, such as ohmic dissipation, Oersted fields, and capacitive time constants. Lateral spin valves (LSVs)[1–5] provide a direct approach to study the generation and transport of pure spin currents. A LSV consists of a non-magnetic wire (NM) connected to two ferromagnets (FM1 and FM2; see Fig. 1). The spin accumulation in the NM is induced by passing a spin-polarized charge current I from FM2 to one end of the NM (C1 → C4). The spin accumulation decays in the NM toward the other end, where no charge current is flowing, and gives rise to a pure spin current, which generates a non-local voltage signal at FM1 (C2 → C3). The voltage difference V_S for parallel and antiparallel alignment of FM1 and FM2, which is controlled by applying an in-plane magnetic field, is a measure of the pure spin current. Therefore, well-defined magnetization reversals of FM1 and FM2 at different external fields in addition to high spin polarization, large spin diffusion length, clean interfaces, and high conductivities are required to achieve strong spin signals. Usually, single-domain-like behavior of the FMs is assumed, e.g., due to shape anisotropy. Multi-domain states and their influence on pure spin currents have not been investigated previously.

Here, we present an *in situ* ultra high vacuum (UHV) fabrication procedure, which leads to lateral spin valves with clean interfaces and high conductivity. We choose the FMs to be on top of the NM, which allows *in situ* imaging the domain structure of all magnetic parts of the completed LSV by scanning electron microscopy (SEM) with polarization analysis (SEMPA). We image the domain structures of LSVs with different dimensions and demonstrate their influence on the spin signal by correlating non-local spin transport measurements with the anisotropic magnetoresistance (AMR) of the FMs and SEMPA images.

The base for our LSVs are two intersecting 50-nm-thick and, near the crossing point, 100-μm-wide polycrystalline Cu lines. They are deposited on an oxidized Si wafer by vapor deposition under a pressure of 7×10^{-10} mbar and capped with a 2-nm-thick Au layer to prevent oxidation. Contact pads at the end of the wires (labeled C1 to C4) are bonded to four contacts on the sample holder to enable *in situ* electrical measurements. All following fabrication and measuring steps are performed in the "Nanospintronics Cluster Tool," a multi-chamber UHV system which houses, among other instrumentation evaporators, SEM/SEMPA, a focused ion beam (FIB), and a four-terminal magnetotransport measurement setup with the magnetic field applied along the axes of the magnetic wires of the LSV. All measurements are performed at room temperature (RT). After removing the Au cap layer by Ar sputtering, FIB is used to narrow down the Cu near the crossing point to a width of 270 nm (NM in Fig. 1) and to remove the Cu in the areas, where the FMs will be located. Subsequently, a 10-nm-thick
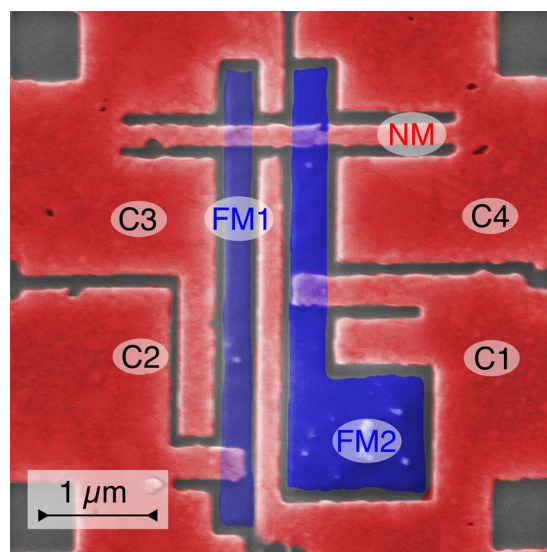

FIG. 1. (Color online) Colored SEM image of an *in situ* fabricated lateral spin valve. FM1 and FM2 denote the vertically running ferromagnetic Co elements, NM the non-magnetic Cu wire in-between, and C1 to C4 the four Cu contacts.

[a]Electronic mail: d.buergler@fz-juelich.de.

polycrystalline Co layer is evaporated through a shadow mask on the crossing region (1×1 mm^2) under a pressure of 2×10^{-10} mbar. FM1 and FM2 are then cut from the Co film in a second FIB structuring step. The shape and size of the magnets was modified in the course of the work and will be specified for each measurement. Figure 1 shows a SEM image of a completed LSV. Co and Cu parts are separated by 100 nm narrow gaps to avoid substrate charging during SEMPA imaging. The FMs are 220 nm $\times$ 4.3 μm (FM1) and 280 nm $\times$ 4 μm (FM2) in size, and the distance between their inner edges is 300 nm, i.e., comparable to the spin diffusion length in Cu.[2] The quadratic pad at the bottom of FM2 facilitating the injection of domain walls as well as the different aspect ratios are designed to yield different coercive fields for FM1 and FM2. Two-terminal resistance measurements evidence ohmic character of the Co/Cu interfaces, and the measured resistivities $\rho_{Co} = 5.26$ $\mu\Omega$cm and $\rho_{Cu} = 1.89$ $\mu\Omega$cm are very close to the bulk literature values and thus indicate the high quality of the LSV and the absence of significant FIB-induced damage in Cu that would give rise to a decreased spin diffusion length.

Figure 2(a) shows a SEMPA measurement of the remanent state of the LSV depicted in Fig. 1. The local magnetization direction obtained from combining two simultaneously measured images revealing magnetization contrast for two orthogonal axes in the sample plane is plotted in false color, and the derived domain pattern is superimposed. In contrast to the single-domain-like behavior expected due to shape anisotropy, both FMs show a rich domain structure. The domains are not correlated with the position of the underlying Cu leads. Therefore, the deviation of the Co magnets from the entirely planar geometry is not the dominant mechanism for domain formation in our samples. We traced the origin of the domains back to the roughness of the wafer surface prior to Co deposition, which is induced by the FIB milling step required to remove the Cu film at the locations of the FMs. The polycrystallinity and the dependence of the sputter yield on the crystal orientation leads to a surface roughness that we estimate from FIB dose series to be of the order of several nm with the typical lateral dimension of 300 nm

corresponding to the in-plane Cu grain size. In order to confirm the roughness hypothesis, we fabricated Co magnets of identical shape and size directly on the Cu surface without the intermediate FIB milling step. In this case [Fig. 2(b)], the magnetization in the narrow parts of the FMs is single-domain-like and a Landau domain structure is visible in the pad of FM2. This observation is consistent with the shape of the FMs and demonstrates that FIB milling causes the multi-domain state in Fig. 2(a). However, the sample shown in Fig. 2(b) is not suitable for electrical measurements, as the Co magnets are shortened by the underlying Cu film.

The magnetic switching behavior of FM1 and FM2 of functioning LSVs is investigated by measuring the AMR of each FM in a two-terminal configuration. The AMR curves of a LSV with rectangular FMs of the same width of 270 nm and different lengths of 2.5 (FM1) and 4 μm (FM2) are shown in Fig. 3. (The offset between positive and negative saturation originates from non-linear thermal drift that is not removed by our linear drift compensation.) Their shapes with different slopes for small and large fields and the sporadic steps are due to a multi-domain state with a distribution of pinning strengths, resulting in a magnetization reversal by rotation rather than a sudden domain wall motion. The AMR ratios reach up to 1 per mille.

The solid and dashed curves in the lower part of Fig. 3 show two runs of non-local electrical four-terminal measurements performed with an AC excitation of $I = 100$ μA amplitude at a frequency of 433 Hz and lock-in detection of V_S. Both measurements yield a spin resistance $R_S = V_S/I \approx 0.9$mΩ at RT, which is among the largest in literature.[6–9] The two R_S levels are usually identified with the parallel and antiparallel alignment of FM1 and FM2. However, as the two displayed measurements demonstrate, the form of the curves is not completely reproducible. For instance, for negative magnetic fields, the configuration corresponding to the lower R_S level is not always detected. Furthermore, the AMR switching fields for the single FMs
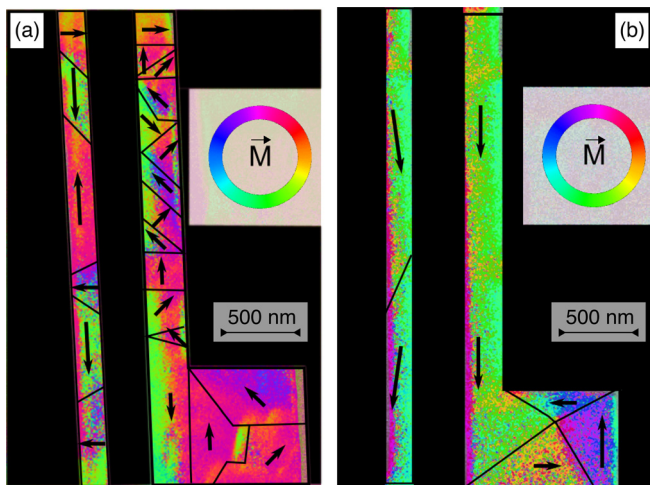

FIG. 2. (Color online) SEMPA images of the domain structure of (a) the LSV depicted in Fig. 1 and (b) a test structure fabricated without substrate roughening due to FIB milling.
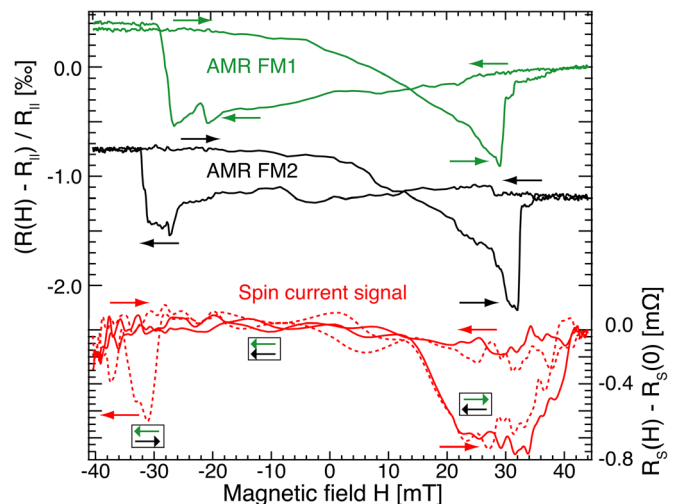

FIG. 3. (Color online) AMR measurements of FM1 and FM2 (vertically offset for clarity) and spin current signal $R_S(H)$ (dotted and solid lines corresponds to two measurement runs) of a LSV with 270-nm-wide FMs. Arrows indicate the field sweep direction. Framed pairs of arrows represent the relative alignment of the magnetizations of FM1 and FM2 at the respective FM/NM interfaces.

(curves labeled AMR FM1 and AMR FM2) do not coincide with the transitions between the two R_S levels. Both features can be explained by magnetic domain structures, as those observed in Fig. 2. For the generation and detection of a pure spin current, only the magnetic configurations in the FM/NM interface areas matter, whereas the AMR signal depends on the magnetization orientation throughout the FMs. Therefore, the framed pairs of arrows in Fig. 3 represent the alignment of the averaged magnetizations in the injection and detection areas. The formation of domains in these areas is not reproducible for successive field cycles and explains the poor reproducibility of the R_S curves. If the injection and detection areas both contain only one domain, it is possible to generate and detect spin accumulation and to observe pure spin currents. If either region contains more than one domain [e.g., FM2 in Fig. 2(a)], they tend to cancel their respective contributions to the spin signal. The existence of domains in the FMs of a LSV has thus strong impact on the R_S signal.

The number of domains in the FMs can be reduced by increasing their widths beyond the lateral size of 300 nm of the FIB-induced roughness. Figure 4 shows SEM and SEMPA images of a LSV with 480 nm (FM1) and 350 nm (FM2) wide FMs. The number and density of domains is clearly reduced. FM1 displays a remanent state similar to the Landau configuration. Most small domains in FM2 reside at a side edge, whereas a large domain extends through the major part of FM2. Hence, we expect rather single-domain-like behavior, which indeed is reflected in the electrical measurements shown in Fig. 5. The AMR curve of FM1 shows a more rectangular profile and a reduced maximal AMR ratio of 0.2 per mille, indicating that the magnetization reversal occurs predominantly in two steps from negative saturation through a Landau-like state for small fields to positive saturation. The shape of the AMR curve of FM2 is comparable to those in Fig. 3; however, the lower number of domains yields a reduced amplitude, as a smaller fraction of the magnetization in FM2 points perpendicular to the current direction. The spin signal (bottom most curve in Fig. 5) now correlates with the AMR curves (dashed lines). The jumps in $R_S(H)$ correspond to changes of the relative magnetization alignment in the
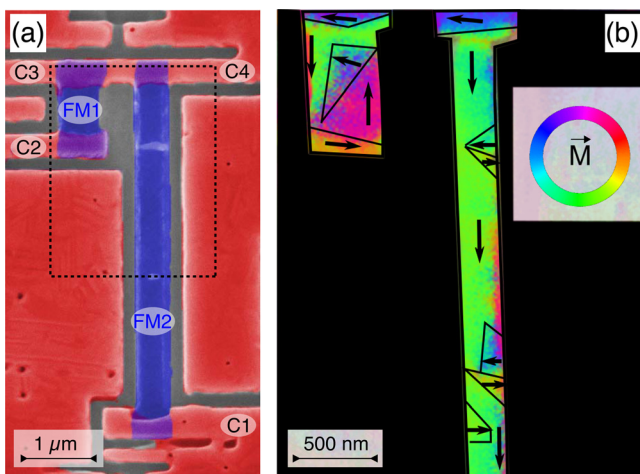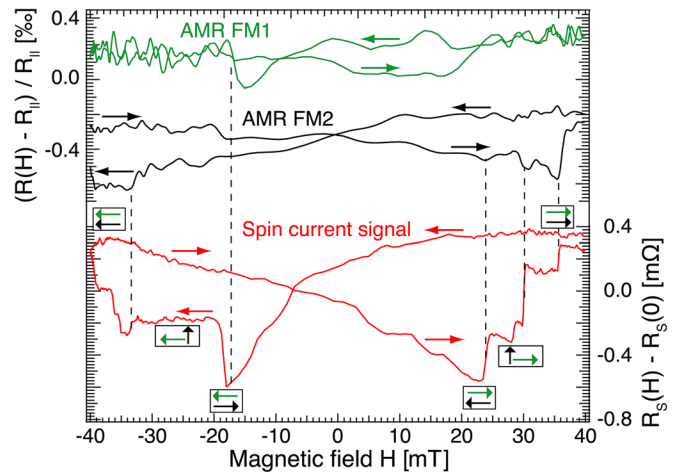

FIG. 5. (Color online) AMR measurements of FM1 and FM2 (vertically offset for clarity) and spin current signal $R_S(H)$ of the LSV shown in Fig. 4. Arrows indicate the field sweep direction. Framed pairs of arrows represent the relative alignment of the magnetizations of FM1 and FM2 at the respective FM/NM interfaces.

injection and detection areas, which also show up in the AMR curves, albeit less pronounced because contributions to the AMR of some remaining domains throughout the magnets are superimposed. The maximum amplitude of R_S is 0.9 mΩ and, thus, equal to Fig. 3.

We attempted to image spin accumulation in the Cu wire with SEMPA. Although we were able to acquire high-resolution images while applying the AC excitation without spurious effects, it was not possible to detect spin accumulation. We estimate the spin accumulation in Cu to be equivalent to a magnetization of 1.4×10^{-4} μ_B, resulting in a spin asymmetry in SEMPA, which is orders of magnitude less than the detection limit of about 1%. Thus, imaging of spin accumulation was not possible for similar reasons as in a recent attempt utilizing circular dichroism in soft x ray microscopy.[10]

In conclusion, the domain structure in LSVs can have a strong impact on the pure spin current. In the extreme case, the generation or detection of spin accumulation is completely impeded, rendering measured spin current amplitudes (R_S) ambiguous. Deviations from single-domain behavior can arise from details of the fabrication process, in our case, FIB-induced substrate roughness, and need to be characterized, e.g., by correlating the spin signal to AMR data or by direct magnetic imaging, as demonstrated here.

FIG. 4. (Color online) (a) SEM image of a LSV with wider FMs: 480 nm × 1 μm for FM1 and 350 nm × 4 μm for FM2. (b) SEMPA image of the area inside the dashed frame in (a).

[1] M. Johnson and R. H. Silsbee, Phys. Rev. Lett. **55**, 1790 (1985).
[2] F. J. Jedema, A. T. Filip, and B. J. van Wees, Nature **410**, 345 (2001).
[3] Y. Ji, A. Hoffmann, J. S. Jiang, and S. D. Bader, Appl. Phys. Lett. **85**, 6218 (2004).
[4] T. Kimura, J. Hamrle, and Y. Otani, Appl. Phys. Lett. **85**, 3501 (2004).
[5] S. O. Valenzuela and M. Tinkham, Appl. Phys. Lett. **85**, 5914 (2004).
[6] T. Kimura and Y. Otani, Phys. Rev. Lett. **99**, 196604 (2007).
[7] T. Yang, T. Kimura, and Y. Otani, Nature Phys. **4**, 851 (2008).
[8] G. Mihajlović, J. E. Pearson, S. D. Bader, and A. Hoffmann, Phys. Rev. Lett. **104**, 237202 (2010).
[9] G. Mihajlović, D. K. Schreiber, Y. Liu, J. E. Pearson, S. D. Bader, A. K. Petford-Long, and A. Hoffmann, Appl. Phys. Lett. **97**, 112502 (2010).
[10] O. Mosendz, G. Mihajlović, J. E. Pearson, P. Fischer, M.-Y. Im, S. D. Bader, and A. Hoffmann, Phys. Rev. B **80**, 104439 (2009).